Journal of Molecular Catalysis B: Enzymatic 99 (2014) 68–78

Contents lists available at ScienceDirect

Journal of Molecular Catalysis B: Enzymatic

journal homepage: www.elsevier.com/locate/molcatb

Kinetic characterization of *Rhodococcus ruber* DSM 44541 alcohol dehydrogenase A

Emil Hamnevik, Cecilia Blikstad, Sara Norrehed, Mikael Widersten*

Department of Chemistry – BMC, Uppsala University, Box 576, SE-751 23 Uppsala, Sweden

ARTICLE INFO

Article history:
Received 8 October 2013
Received in revised form 30 October 2013
Accepted 30 October 2013
Available online 7 November 2013

Keywords:
Alcohol dehydrogenase
Kinetic mechanism
Pre-steady state kinetics
Product inhibition

ABSTRACT

An increasing interest in biocatalysis and the use of stereoselective alcohol dehydrogenases in synthetic asymmetric catalysis motivates detailed studies of potentially useful enzymes such as alcohol dehydrogenase A (ADH-A) from *Rhodococcus ruber*. This enzyme is capable of catalyzing enantio-, and regioselective production of phenyl-substituted α-hydroxy ketones (acyloins) which are precursors for the synthesis of a range of biologically active compounds. In this study, we have determined the enzyme activity for a selection of phenyl-substituted vicinal diols and other aryl- or alkyl-substituted alcohols and ketones. In addition, the kinetic mechanism for the oxidation of (*R*)- and (*S*)-1-phenylethanol and the reduction of acetophenone has been identified as an Iso Theorell–Chance (hit and run) mechanism with conformational changes of the enzyme-coenzyme binary complexes as rate-determining for the oxidation of (*S*)-1-phenylethanol and the reduction of acetophenone. The underlying cause of the 270-fold enantiopreference for the (*S*)-enantiomer of 1-phenylethanol has been attributed to non-productive binding of the *R*-enantiomer. We have also shown that it is possible to tune the direction of the redox chemistry by adjusting pH with the oxidative reaction being favored at pH values above 7.

1. Introduction

In cells, NAD(P)H-dependent reactions, catalyzed by dehydrogenases (EC 1.1.1.1), are instrumental in all aspects of metabolism. The coenzymes act as carriers of reductive power affording energy transformations and biosynthesis. The spectroscopic signals, changes in absorption or fluorescence, reflecting the redox state and local environment of the coenzyme provide sensitive and selective probes of discrete reaction steps during catalysis. This has enabled gathering of an immense volume of experimental data describing various aspects of dehydrogenase functions. Hence, these reactions have been applied as model systems in studies of fundamental enzymology since the beginning of the research field [1], also increasing our understanding of enzyme-afforded catalysis in general. Typical NAD(P)H-dependent reactions involve reduction of carbonyl compounds (ketones or aldehydes) into the corresponding secondary or primary alcohols, respectively. The carbonyl carbon of a substituted ketone is prochiral and its reduction will therefore result in a chiral product. This added structural complexity requires stereoselective substrate recognition of the cognate enzyme catalysts (Scheme 1A).

Stereoselectivity is a key feature also in asymmetric catalysis applied to synthetic chemistry. There is therefore an increasing interest in applying stereoselective dehydrogenase enzymes as biocatalysts in reversible oxidation/reduction of alcohols and ketones [2–10]. We are exploring possibilities to exchange traditional organic and organometallic catalysis with biocatalysis to afford synthesis of chiral and prochiral compounds. The starting materials are aryl-substituted epoxides which are hydrolyzed to yield chiral vicinal diols in reactions catalyzed by epoxide hydrolase (Scheme 1B) [11–13]. The diol products may subsequently be derivatized further. Oxidation of a secondary alcohol produces the corresponding α-hydroxy ketone (acyloin). Acyloins are important building blocks for the synthesis of a range of biologically active compounds such as anti-depressants, inhibitors of amyloid protein production and anti-tumor antibiotics [14].

Alcohol dehydrogenase A (ADH-A) from *Rhodococcus ruber* DSM 44541 catalyzes the reversible reduction/oxidation of ketones and *sec*-alcohols, respectively [15,16]. The enzyme is a classical zinc-dependent group I alcohol dehydrogenase [17,18] structurally similar to the, in detail studied, horse liver isoenzyme [19,20]. ADH-A displays favorable physicochemical properties, such as tolerance to high concentrations of isopropanol and acetone [21] which allows for facile cofactor regeneration. In addition, ADH-A catalyzes the oxidation of bulky aryl-substituted alcohols and was therefore considered a good candidate catalyst for the oxidation of vicinal diols as outlined in Scheme 1B. Our aims with

* Corresponding author. Tel.: +46 18 471 4992; fax: +46 18 55 8431.
E-mail address: mikael.widersten@kemi.uu.se (M. Widersten).

1381-1177/$ – see front matter © 2013 Elsevier B.V. All rights reserved.
http://dx.doi.org/10.1016/j.molcatb.2013.10.023

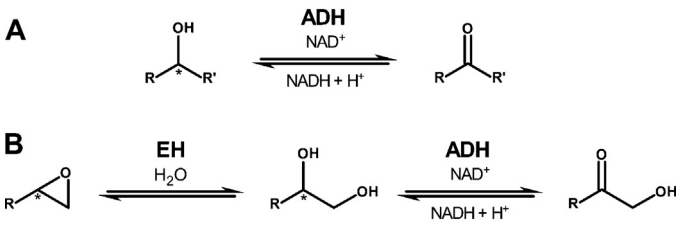

Scheme 1. (A) Scheme of a generic dehydrogenase catalyzed oxidation of a *sec*-alcohol into the corresponding ketone. (B) Mini-pathway of enzyme-catalyzed synthesis of acyloins from substituted epoxides. An asterisk indicates a chiral center. EH, epoxide hydrolase, ADH, alcohol dehydrogenase.

the present work were as follows: (1) to establish the substrate-, enantio-, and regioselectivities of ADH-A regarding oxidation of aryl-substituted vicinal diols and other alcohol and ketone substrates (Fig. 1), (2) to characterize the kinetic mechanism of the enzyme. The gathered information will form the baseline guiding future directed-evolution efforts aiming to generate more efficient biocatalysts for synthesis of new acyloins and other substituted ketones.

2. Experimental

2.1. Chemicals and reagents

Standard reagents for protein expression and all enzyme substrates (except **10**) were purchased from Sigma–Aldrich, Merck and VWR. The (*S*)- and (*R*)-3-phenyl-1,2-propane diols (**10**) were obtained after enzyme-catalyzed hydrolysis of the corresponding (*S*)- and (*R*)-benzyloxiranes (Tokyo Chemical Industry Co) according to the protocol in ref. [11]. Restriction enzymes DNA polymerases and other DNA modifying enzymes were purchased from Fermentas.

2.2. ADH-A gene cloning

The gene sequence encoding alcohol dehydrogenase A (ADH-A) from *R. ruber* DSM 44541 was optimized for expression in *Escherichia coli*, synthesized and purchased from Invitrogen using their GeneArt® service. The final gene construct was flanked by the restriction sites for *Xho*I and *Spe*I at the 5′- and 3′-ends of the gene, respectively. The gene was subcloned into a modified pGT7YNR064c-5H vector [22] (inserting codons for a penta-histidyl tag at the 3′-end of the open reading frame) using *Xho*I and *Spe*I. An unwanted *Bam*HI site present in the vector was removed by Klenow fill-in prior to subcloning of the ADH-A synthetic gene. The formed construct was denoted as pGT7ADHA-5H. The ADH-A gene was sequenced in full to ensure sequence integrity.

2.3. Site-directed mutagenesis of His39 to Asn

His39 was mutated into an Asn by site-directed mutagenesis using the QuikChange method (Agilent Technologies). The mutation was inserted into pGT7ADHA-5H using PCR in the presence of the following mutagenic primers: (Fwd His39Asn) CTG TGT *AAT* AGC GAT ATT TTT GTT ATG GAT ATG CCT GCA GCA CAG and (Rev His39Asn) C GCT *ATT* ACA CAG ACC TGC TGC GGT AAC TTT CAG CAG AAT TTC. The product was purified and digested with *Dpn*I after which it was transformed into electrocompetent *E. coli* XL1-blue cells by electroporation. The H39N expression construct was purified and the ADH-A H39N gene was sequenced in full to ensure that no unwanted mutations had been introduced.

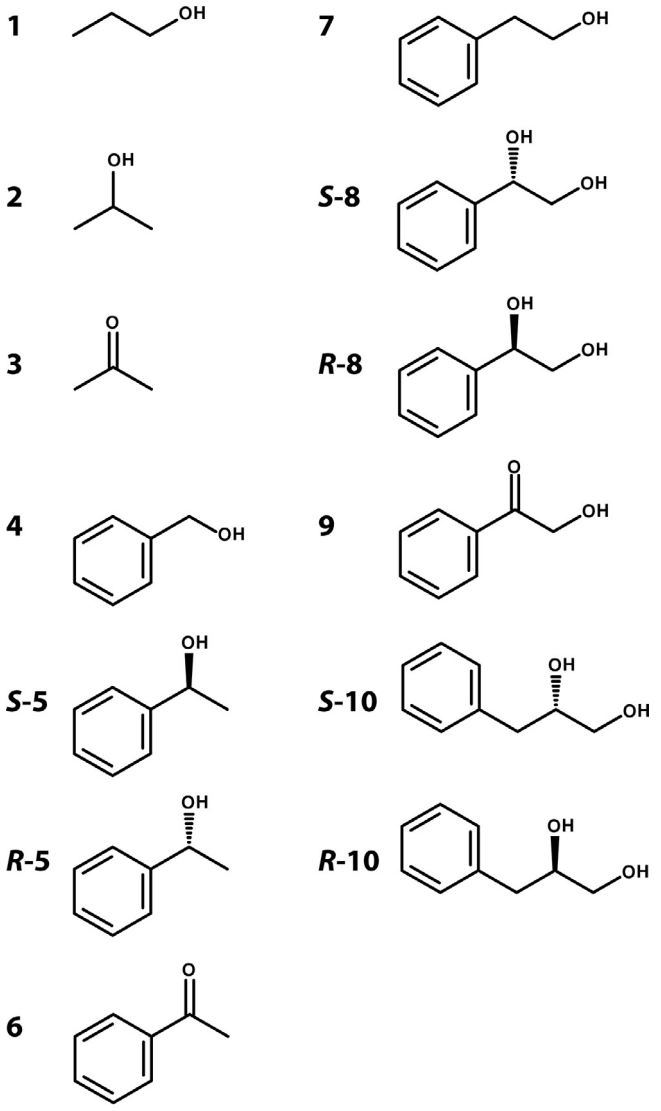

Fig. 1. Alcohols and ketones tested as substrates. **1**, 1-propanol, **2**, 2-propanol, **3**, acetone, **4**, benzyl alcohol, **5**, 1-phenylethanol, **6**, acetophenone, **7**, 2-phenylethanol, **8**, 1-phenyl-1,2-ethanediol, **9**, 2-hydroxyacetophenone, and **10**, 3-phenyl-1,2-propanediol.

2.4. Protein expression and purification

The expression constructs were transformed into chemically competent *E. coli* BL21-AI cells (Invitrogen) pre-transformed with the expression plasmid pREP4-groEL/ES [23] allowing for concomitant over-expression of chaperonins GroEL/ES. BL21-AI cells containing pGT7ADHA-5H, or the corresponding construct encoding the H39N mutant, (and pREP4-groEL/ES) were incubated in 2 ml 2TY media (1.6% (w/v) tryptone, 1.0% (w/v) yeast extract, 0.5% (w/v) NaCl) containing 100 μg/ml ampicillin and 30 μg/ml kanamycin at 30 °C for 6 h. The culture was subsequently diluted 1:50 in 50 ml 2TY containing 100 μg/ml ampicillin and 30 μg/ml kanamycin and incubated for additional 16 h at 30 °C. Finally, the culture was diluted 1:100 in 6 × 500 ml 2TY containing 50 μg/ml ampicillin and 15 μg/ml kanamycin and incubated at 30 °C until an OD_{600} of 0.4 was reached (approximately 2.5 h). Expressions of the ADH-A and GroEL/ES genes were induced by addition of 0.2% (w/v) L-arabinose and 1 mM isopropyl β-D-1-thiogalactopyranoside, respectively. The culture was incubated for additional 3 h at 30 °C. Cells were

harvested by centrifugation at 3800 × *g* for 13 min at 4 °C. Bacteria were resuspended in 20 ml Binding Buffer (20 mM sodium phosphate, 20 mM imidazole, 500 mM NaCl, 0.02% sodium azide, pH 7.5) fortified with protease inhibitors (EDTA-free Complete, Roche) and 20 μg/ml DNaseI. Cells were lysed using a Cell disruptor Z plus series (Constant Systems LTD) and debris was removed by centrifugation at 27,200 × *g* for 1 h at 4 °C. The supernatant was transferred to a conical 50 ml tube and 2.5 ml Ni^{2+}-immobilized metal ion affinity chromatography (IMAC) gel solution (Chelating Sepharose™ fast flow, GE Healthcare) equilibrated with Binding Buffer (75% v/v gel) was added to the lysate and the slurry was incubated at 4 °C for 1 h. The gel/lysate slurry was subsequently centrifuged at 100 × *g* at 4 °C and the supernatant was discarded. Washing Buffer (Binding Buffer containing 100 mM imidazole) was added to a total volume of 20 ml and gel slurry was incubated at 4 °C for 10 min before centrifuged as above. The washing step was repeated two additional times. Elution of ADH-A was achieved by adding 5 ml of Elution buffer (Binding Buffer containing 300 mM imidazole) to the IMAC gel. The gel slurry was transferred to a conical 15 ml tube and incubated for 20 min at 4 °C. The gel–buffer mix was centrifuged at 140 × *g* at 4 °C and the supernatant was transferred to a new 15 ml conical tube. This elution step was performed twice. The eluted fractions were pooled and concentrated down to 2.5 ml using a spin-column (Vivaspin 20, 10,000 M_W cut-off, Sartorius Stedim Biotech). The concentrated sample was desalted using a PD-10 column (GE Healthcare) equilibrated with Desalting Buffer (0.1 M sodium phosphate, 10 μM $ZnSO_4$, 0.02% sodium azide, pH 7.4) according to the manufacturer's protocol. The purified enzyme sample was stored at 4 °C. Enzyme purity was controlled by SDS–PAGE and staining with Coomassie Brilliant Blue R-250. The molar extinction coefficient at 280 nm was determined to be 31,500 cm^{-1} M^{-1} by measuring the absorbance in a UV-1700 Pharmaspec UV–vis spectrophotometer (Shimadzu) with a concomitant determination of the ADH-A concentration by quantitative amino acid analysis.

2.5. Steady state kinetics

Steady state kinetic parameters for ADH-A, or the H39N mutant, were obtained by measuring initial velocities in the presence of varying concentrations of 1-propanol (**1**, Fig. 1), 2-propanol (**2**), acetone (**3**), benzyl alcohol (**4**), (*S*)-1-phenylethanol (*S*-**5**), (*R*)-1-phenylethanol (*R*-**5**), acetophenone (**6**), 2-phenylethanol (**7**), (*S*)-1-phenyl-1,2-ethanediol (*S*-**8**), (*R*)-1-phenyl-1,2-ethanediol (*R*-**9**), 2-hydroxy acetophenone (**9**), (*S*)-3-phenyl-1,2-propanediol (*S*-**10**), (*R*)-3-phenyl-1,2-propanediol (*R*-**10**), and in the presence of saturating concentrations of NAD^+ or NADH. All reactions were performed in 0.1 M sodium phosphate, pH 8.0 at 30 °C and 1% (v/v) acetonitrile. Final concentrations were 6–100 mM **1**–**3**, 1.8–30 mM **4**, 0.11–7.5 mM *S*-**5**, 0.3–10 mM *R*-**5**, 0.1–7 mM **6**, 0.38–12.5 mM **7**, 1.7–28 mM *S*-**8**, 0.1–28 mM *R*-**8**, 0.18–12.5 mM **9**, 0.1–50 mM *S*-**10** and *R*-**10**, in the presence of 1.6 mM NAD^+ (18 × K_m) in the oxidation of alcohols and 0.4 mM NADH (10 × K_m) when reducing ketones. The kinetic parameters in the presence of varied concentrations of coenzymes were determined in 0.015–1.6 mM NAD^+ and 7.5 mM *S*-**5** (12 × K_m) and 0.005–0.4 mM NADH and 5 mM **6** (4.2 × K_m). Reduction of NAD^+ or oxidation of NADH was monitored at 340 nm in a UV-1700 Pharmaspec UV–vis spectrophotometer (Shimadzu). The kinetic parameters, k_{cat} and K_m were extracted after fitting the Michaelis–Menten equation by non-linear regression to the initial velocity data with program MMFIT (in the SIMFIT package, www.simfit.uk.org) and k_{cat}/K_m was determined from the same raw data after fitting the equation $v_0 = ((k_{cat}/K_m)[S])/(1 + [S]/K_m)$ with program RFFIT.

2.6. Zinc-dependent functional integrity

Purified ADH-A was stored at 4 °C in either Desalting Buffer or Desalting Buffer devoid of $ZnSO_4$ during 40 and 60 days, respectively. Aliquots were removed at different time intervals and remaining enzyme activity was determined. Initial reaction velocities were measured in 0.1 M sodium phosphate, pH 7.0 at 30 °C and 1% (v/v) acetonitrile with final concentrations of 5 mM acetophenone and 0.4 mM NADH.

2.7. pH-dependence of enzyme activity

The pH dependencies of k_{cat} and k_{cat}/K_m for wt ADH-A and ADH-A H39N-catalyzed oxidation of *S*-**5** and reduction of **6** were determined in the pH range of 5–9. Reactions were performed in 96-well polystyrene plates (Nunc) in 0.1 M sodium phosphate (pH 5–8.5) or 0.1 M glycine (pH 8.5–9.0) at 30 °C and 1% (v/v) acetonitrile with final concentrations of 0.2–7.5 mM *S*-**5** and 1.6 mM NAD^+ in the oxidation reactions and, 0.18–7.0 mM **6** and 0.4 mM NADH in the reduction reactions. Reduction or oxidation of the coenzyme was monitored at 340 nm in a Spectra MAX 190 UV–vis spectrophotometer (Molecular Devices) using an extinction coefficient for NADH of 3440 M^{-1} cm^{-1}. Kinetic parameters were determined as described above. Apparent acid constants were extracted by fitting expressions for titration of one- or two-proton systems (Equations (1) and (2), respectively), where L_H is the titrated parameter k_{cat} or k_{cat}/K_m. The extra parameters for a two-proton system were only included if justified by an F-test. Curve fitting was performed with program RFFIT in SIMFIT.

$$L_H = \frac{L_{HA}[H^+] + L_{A-}K_{a1}}{K_{a1} + [H^+]} \quad (1)$$

$$L_H = \frac{L_{H2A}[H^+]^2 + L_{HA-}[H^+]K_{a1} + K_{a1}K_{a2}L_{A2-}}{K_{a1}K_{a2} + [H^+]K_{a1} + [H^+]^2} \quad (2)$$

2.8. Product inhibition

The steady state kinetics was analyzed in the presence of increasing concentrations of either product (**6** and NADH) in the oxidative direction *i.e.* *S*-**5** oxidation and NAD^+ reduction. Measurements were performed as described above in the paragraph describing the steady state kinetics measurements. Final concentrations of alcohol were 0.12–7.5 mM, and 1.6 mM NAD^+ and 0–0.2 mM NADH or 0–3 mM **6**. Final concentrations for coenzyme reduction were 0.015–3.6 mM NAD^+ with 7.5 mM *S*-**5** and 0–0.12 mM NADH or 0–5 mM **6**. The Michaelis–Menten equation was fitted to the velocity data using MMFIT and the fits were graphically presented as double-reciprocal plots.

2.9. Regioselectivity

R-**5** or *S*-**5** (60 mM) were mixed with 1.6 mM NAD^+, 60 mM sodium pyruvate, 2 U/ml L-lactic dehydrogenase (Sigma) and 3 μM of ADH-A in 0.1 M ammonium bicarbonate to a total volume of 10 ml. The reactions were incubated at 30 °C for 10 h in the dark. $CDCl_3$ (2.4 ml) was added to each reaction vial, forming a two-phase system. The phases were mixed by vortexing for 5 s and were subsequently allowed to separate. The $CDCl_3$ phases were transferred to new vials. Aliquots from the $CDCl_3$ phases were analyzed by reverse phase HPLC on an Ascentis C-18 column (Supelco, 25 cm × 4.6 mm, 5 μm) using an isocratic elution of 37% (v/v) methanol in water and 0.1% (v/v) of formic acid.

NMR investigations of the reaction products were carried out on a Varian Unity Inova (^1H at 499.94 MHz, ^{13}C at 125.7 MHz)

spectrometer. Chemical shifts were reported in ppm referenced to tetramethylsilane via the residual solvent signal ($CDCl_3$, ^1H at 7.26 and ^{13}C at 77 ppm). Signal assignments were derived from gHSQC [24], gHMBC [25], and TOCSY [26] spectra.

2.10. Pre-steady state kinetics

Transient kinetics experiments were performed on an Applied Photophysics (Leatherhead, UK) SX.20MV sequential stopped-flow spectrophotometer/fluorometer. All measurements were performed at 30 °C in 0.1 M sodium phosphate, pH 8.0. Averages of 8–10 progression curves were used in all cases and the apparent rates, k_{obs}, were determined by fitting Equation (3), a function of a single exponential with floating endpoint, to the progression curves. F is the recorded fluorescence signal, A, the signal amplitude, t, time and C, the floating end point.

$$F = A\exp(-k_{obs}t) + C \quad (3)$$

2.10.1. Coenzyme binding

Binding of coenzyme to ADH-A was detected by monitoring the change in intrinsic protein tryptophan fluorescence which occur upon binding of NADH/NAD^+ to the enzyme active site. An excitation wavelength of 290 nm was used and fluorescence light was collected through a 320 nm cut-off filter. Concentration of NADH ranged from 10 to 75 μM and for NAD^+ from 1.7 to 67 μM. Enzyme concentrations for NADH measurements were between 0.8 and 2.2 μM and for NAD^+ measurements between 0.14 and 1.1 μM. Nucleotide concentrations were always kept in at least 10-fold excess as compared to the enzyme concentrations. The apparent rates, k_{obs}, were determined as described above. The kinetic parameters were determined by fitting the dependence of k_{obs} on the coenzyme concentration to a linear (Equation (4)) or a hyperbolic function (Equation (5)) using LINFIT or QNFIT, respectively. Model discrimination was decided from F-tests of the fitting results with an accepted significance level of $p \leq 0.05$.

$$k_{obs} = k_{on}[NAD(H)] + k_{off} \quad (4)$$

$$k_{obs} = \frac{k_f[NAD(H)]}{K_S^{NAD(H)} + [NAD(H)]} + k_r \quad (5)$$

2.10.2. The redox chemistry

The alcohol oxidation was monitored by following the change in fluorescence upon increase (alcohol oxidation) of the NADH concentration. Change in fluorescence was detected using an excitation wavelength of 340 nm and collecting the fluorescent light after passage through a 395 nm cut-off filter. The oxidation reaction was measured with *S*-**5** and *R*-**5** with NAD^+ as electron acceptor. For measurements with *S*-**5** the substrate concentrations varied between 0.6 and 10 mM and the enzyme concentration was 0.6 μM. For *R*-**5**, the substrate concentrations were varied between 1.5 and 10 mM and the enzyme concentration was 2.3 μM. In both cases [NAD^+] was kept constant at 0.4 mM. Before measurements, the fluorescence of the NAD^+-enzyme complex was monitored and the voltage was thereafter adjusted to 8.0 V. Averaged progression curves were fitted to the function of single exponential with floating endpoint, as described above, to determine the apparent rates, k_{obs}. The kinetic parameters, k_4 and K_3 were extracted by fitting the obtained rates to Equation (6) by non-linear regression using MMFIT.

$$k_{obs} = \frac{k_4[alcohol]}{K_3 + [alcohol]} \quad (6)$$

3. Results and discussion

3.1. Substrate-, enantio- and regioselectivity

It has been shown previously that *R. ruber* ADH-A accepts a broad range of secondary alcohols and ketones as substrates and a wide variety of reaction conditions and co-solvent systems have been tested to assess the potential of this enzyme as a biocatalyst of redox reactions [15,16,27–33]. Our aim with the current work was to complement this already present bulk of important applied data by conducting a detailed kinetic characterization. We have determined the steady state kinetic parameters for a range of aliphatic and aryl-substituted alcohols, diols and ketones in order to provide a quantitative assessment of the enzyme's substrate preferences (Table 1). Our main motivation for the study was to assess the suitability and potential of this enzyme to act as a catalyst for the oxidation of vicinal diols into the corresponding acyloins (cf. Scheme 1B) The data shows that ADH-A strongly prefers secondary alcohols over primary as demonstrated by the ratio of 5000 in the k_{cat}/K_m values for *S*-**5** and **7**. ADH-A also catalyzes the oxidation reaction at pH 8.0, with a 4-fold higher catalytic efficiency as compared to the reduction direction, as seen from a comparison of the catalytic efficiencies with *S*-**5** and **6**. Furthermore, the enzyme prefers bulkier phenyl-substituted substrates over smaller aliphatic compounds as shown by comparing the enzyme efficiencies with **2** and *S*-**5** where k_{cat}/K_m drops 170-fold going from *S*-**5** to **2**, the same behavior is observed if comparing **1** and **7**, or **3** and **6**. The phenyl substituent is assumed to improve both affinity and selectivity in binding to the enzyme active site during formation of a productive ternary complex. One parameter that supports this notion is K_m, which is affected by binding affinity. $K_m^{\mathbf{2}}$ is a 100-fold larger as compared to $K_m^{S\text{-}\mathbf{5}}$ while the respective turnover numbers are comparable suggesting poorer binding of isopropanol at the active site by approximately 3 kcal/mol.

A major reason for the choice of *R. ruber* ADH-A as model enzyme was its putative catalytic function with aryl-substituted vicinal diols. We therefore tested diols **8** and **10** which can be considered hydrolysis products of styrene oxide and (2,3-epoxypropyl)benzene. ADH-A does indeed display activity with these vicinal diols but with lower efficiencies as compared to monohydroxy substituted derivatives; ADH-A displays 2900-fold higher catalytic efficiency with *S*-**5** as compared to *R*-**8**, which is the stereochemically related diol. The probable reason for this decrease in activity is simply steric hindrance and introduction of a polar group by the primary alcohol. The same pattern is observed if comparing the enzyme activities with ketones **6** and **9**, although the effect is less dramatic. The activities with diols *R*/*S*-**10** are 3–10-folds higher as compared to the corresponding **8** enantiomers. A reason may be that the introduction of the extra methylene group in **10** provides increased flexibility in the enzyme–substrate interactions, as compared to the more rigid structure of diol **8**, facilitating formation of productive ternary complexes.

When comparing the substrate selectivities of ADH-A from *R. ruber* with that of horse liver alcohol dehydrogenase [34–37] it is clear that both enzymes are able to catalyze oxidation of primary and secondary alcohols, aliphatic and aryl-substituted alcohols. The two isoenzymes, however, do display differences in their substrate preferences. The horse liver enzyme prefers small primary alcohols, while ADH-A shows highest activity with bulkier secondary alcohols. ADH-A is also more efficient in catalyzing diol oxidations as compared to the horse liver enzyme [37]. These differences can be explained by the respective active-site structures (Fig. 2A). The horse enzyme active site is more narrow, restricted and channel-like while the active site of the *Rhodococcus* isoenzyme forms an open cleft allowing for binding of bulkier substrates

Table 1
Substrate selectivity. Steady state kinetic parameters for ADH-A catalyzed redox reactions with a panel of alcohols and ketones. See Fig. 1 for chemical formulas. Enantioselectivity, *E*, was calculated from the ratios of k_{cat}/K_m for the respective enantiomers. Values refer to the preferred substrate enantiomer with the configuration shown within brackets. Data for the H39N mutant of ADH-A have been included for comparison.

Substrate	k_{cat} (s^{-1})	K_m (mM)	k_{cat}/K_m (s^{-1} mM^{-1})	*E* (fold)
1-propanol (**1**)	–	–	0.0055 ± 0.0002	
2-propanol (**2**)	56 ± 2	74 ± 6	0.76 ± 0.03	
Acetone (**3**)	–	–	0.54 ± 0.02	
Benzyl alcohol (**4**)	0.022 ± 0.001	13 ± 2	0.0018 ± 0.0001	
S-1-phenylethanol (*S*-**5**)	80 ± 20 (H39N: 61 ± 0.8)	0.63 ± 0.05 (H39N: 1.7 ± 0.06)	130 ± 30 (H39 N: 36 ± 0.9)	270 (*S*)
R-1-phenylethanol (*R*-**5**)	0.45 ± 0.005	0.94 ± 0.04	0.48 ± 0.01	
Acetophenone (**6**)	36 ± 0.8 (H39N: 15 ± 0.6)	1.2 ± 0.09 (H39N: 1.2 ± 0.1)	30 ± 2 (H39N: 12 ± 0.9)	
2-phenylethanol (**7**)	0.025 ± 0.00007	0.97 ± 0.1	0.026 ± 0.002	
S-1-phenyl-1,2-ethanediol (*S*-**8**)	0.0094 ± 0.0005	3.0 ± 0.7	0.0031 ± 0.0006	14 (*R*)
R-1-phenyl-1,2-ethanediol (*R*-**8**)	0.73 ± 0.01	17 ± 0.6	0.044 ± 0.0008	
2-hydroxy acetophenone (**9**)	2.0 ± 0.08	3.7 ± 0.4	0.55 ± 0.03	
S-3-phenyl-1,2-propanediol (*S*-**10**)	0.15 ± 0.001	3.0 ± 0.09	0.053 ± 0.001	2.3 (*R*)
R-3-phenyl-1,2-propanediol (*R*-**10**)	0.56 ± 0.005	4.4 ± 0.2	0.12 ± 0.003	
NAD^+	110 ± 10(H39N: 38 ± 0.2)	0.086 ± 0.006(H39N: 0.083 ± 0.002)	1200 ± 200(H39N: 450 ± 9)	
NADH	37 ± 0.5	0.039 ± 0.002	950 ± 40	

(Fig. 2B). The kinetic parameters for reactions with different enantiomers of alcohols used in this study show a preference of ADH-A for the *S*-enantiomer comparing *S*- and *R*-**5**, as have been reported previously [16], with an *E*-value of 270. In the oxidation of diols *R*/*S*-**8** and *R*/*S*-**10** ADH-A shows a preference for the *R*-enantiomer with *E*-values of 14 and 2.3, respectively. The reason for the apparent shift in enantiopreferences, from *S*-preference to *R* for the diols, is due to the change in priority order of substituents resulting from the extra hydroxyl group; the actual configuration of the reacting functional groups is identical. The preference for oxidation of the secondary alcohol of the *R*-**8** vicinal diol was confirmed both by the migration of the product in an HPLC reverse phase system in which 2-hydroxy acetophenone was included as control substance (Fig. SI1 Supplementary Information) and by NMR. NMR studies of the product resulted in signals also supporting 2-hydroxy acetophenone as the only reaction product. The NMR analysis of the oxidation reaction of *S*-**8** was unable to detect any ketone, only starting material was present, probably due to the low turnover number of the enzyme with this substrate (Table 1). Chemical shifts and assignments are presented in the Supplementary Information.

3.2. pH-dependence of catalysis

The catalytic activity, expressed as k_{cat} or k_{cat}/K_m, increases with increasing pH in the oxidation reaction, but decreases with increasing pH in the reduction reaction (Fig. 3). At pH 8, which is the assay pH during the survey of substrate selectivity and the pre-steady state kinetics, the oxidation reaction is favored. The shift in reaction direction preference, from reduction to oxidation, occurs at pH 7.2 for k_{cat} and 6.2 for k_{cat}/K_m. The catalyzed oxidation of *S*-**5** displays a higher degree of pH dependency than does the reduction of ketone **6**. In order to model the titration profiles of k_{cat} and k_{cat}/K_m a two-proton model had to be invoked in the cases of $k_{cat}^{\mathbf{6}}$ and $(k_{cat}/K_m)^{S\text{-}\mathbf{5}}$ (Table 2). The values of pK_{a1} ranges from 6.2 to 7.3, thus, indicating a role for a histidine residue in the rate-limiting catalytic steps of the wild-type enzyme. By looking at the structure of ADH-A (Fig. 2E) and comparing it to the proposed mechanism for proton relay in the horse liver enzyme [38], His39 was considered to be a candidate. Although His39 do not have exactly the same position as His51 in the horse liver enzyme, it can be aligned in a putative proton relay in the *Rhodococcus* enzyme.

To determine if His39 is (partly) responsible for the pH-profiles a H39N mutant was constructed and characterized. The rationale to mutate His39 into an Asn, was to retain the hydrogen bonding interaction between the N-δ of His39 and the pyrophosphate moiety of the bound nucleotide (Fig. 2E) by the amide nitrogen, but to remove the expected positive charge of the protonated imidazolium at lower pH. The effects on the pH-dependence, however, were not dramatic (Fig. 3, Table 2) although the mutation did cause changes in the apparent pK_a values. The pK_a values determined for k_{cat}/K_m were shifted by approximately 1.7 and 1 pH units towards more basic values for the oxidation and reduction reactions, respectively. The effects on k_{cat} for either reaction were modest. Even though the effect on the pK_a values is relatively small, the change in the shapes of the pH-profiles indicates that His39 is indeed contributing to the titration of the wild-type enzyme and may be involved in a proton relay similar to His51 in the horse liver enzyme.

3.3. Kinetics of ADH-A H39N

The ADH-A H39N mutant exhibited a slight decrease in k_{cat} and an increase of 2.7-fold in K_m with *S*-**5** (Table 1, values in brackets), resulting in a 3.6-fold decrease in k_{cat}/K_m. For NAD^+, the K_m was unaffected, but the k_{cat} and k_{cat}/K_m values were decreased by 2.9- and 2.7-fold, respectively. These values, however, should be viewed as apparent and represent lower limit values, since the increase in $K_m^{S\text{-}\mathbf{5}}$ prevents the enzyme to become fully saturated with *S*-**5** during these measurements.

According to the crystal structure (Fig. 2E), His39 line the edge of the nucleotide binding site and interacts directly with the nucleotide. So the fact that the H39N mutation caused no effect on the K_m for NAD^+ is noteworthy and indicates that the replacing amide side-chain can substitute well for the N-δ of His39. The main effect by the mutation was the 3-fold increase in K_m for *S*-**5** by the mutation which may indicate a cross-talk between the two binding sites, may be affected by some small change in the orientation of the bound nucleotide caused by the mutation.

3.4. Zinc-dependence

ADH-A depends on two zinc ions, one catalytic and one structural. At least one of these ions, although we have not identified which one, is not tightly bound to the enzyme but appears to be equilibrated with solution ions. Incubating ADH-A over a period of time in a zinc-free buffer resulted in a decrease of activity over time (Fig. 4). In the experiment without added zinc the enzyme concentration was 40 μM and under these conditions the relative activity leveled off at 50%. When incubated over the same time range in buffer fortified with 10 μM zinc sulfate, the enzyme was practically stable retaining 90–95% of initial activity.

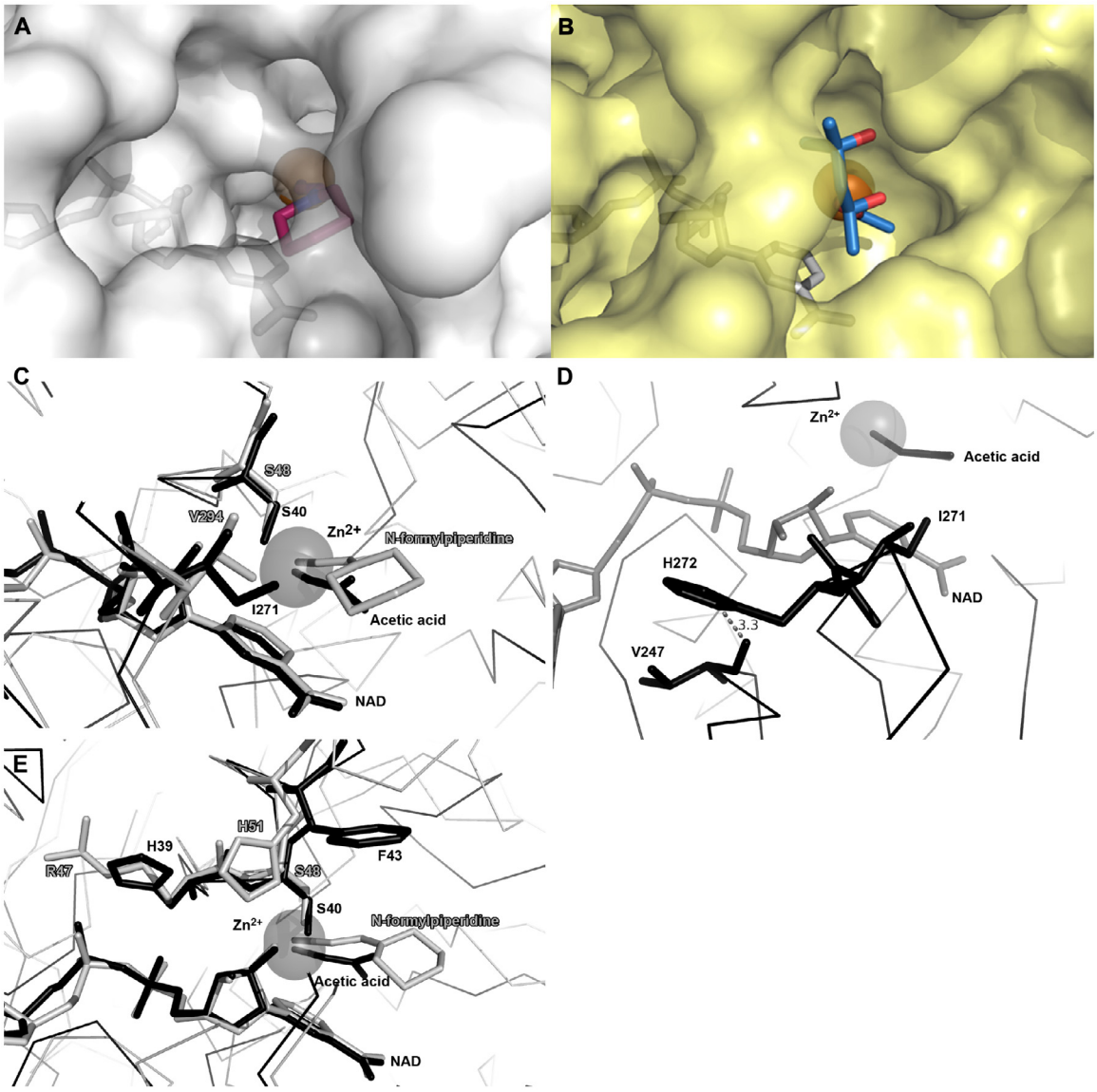

Fig. 2. Structure comparisons between *R. ruber* ADH-A and horse liver ADH. The active-site entry is more restricted in the horse liver enzyme (A) as compared to the *R. ruber* ADH-A (B) explaining the wider substrate scope of the latter. The ligands shown in stick are in (A) N-formyl piperidine and in (B) (4*S*)-2-methyl-2,4-pentanediol. The NAD^+ cofactor is also shown in stick representation. (C) The active-site loops in the "closed̈conformation of the horse liver enzyme (gray) and the *R. ruber* enzyme (black). The functionality of Val294, which is in van der Waals contact with the nicotinamide ring in this conformation, is conserved in Ile271 in the bacterial enzyme. (D) The interaction between the non-conserved His272 and the main-chain carbonyl oxygen of Val247 may contribute to stabilization of the closed conformation of the ADH-A enzyme. (E) His39 in *R. ruber* ADH-A is replaced by Arg47 in horse liver ADH. Both these residues interact with the coenzyme through electrostatic and hydrogen bonds. Image was created with Pymol 1.5 (www.pymol.org) from the atomic coordinates in 1lde [46] for the horse liver enzyme and 3jv7 [20] for the ADH-A structure.

3.5. Kinetic mechanism

The data suggests a Theorell–Chance (hit-and-run) mechanism (Fig. 5B), as was proposed for the horse liver enzyme [39] with a low degree of ternary complex accumulation during the steady state. This is based on the product inhibition patterns, determined at pH 7.0 (Table 3, Fig. 6A), in which NADH (Q) acts as a *competitive inhibitor* of NAD^+ (A) and **6** (P) acts as a competitive inhibitor of *S*-**5** (B) (Fig. SI2). In an ordered Bi Bi mechanism with an accumulation of the ternary EAB complex, which has also been invoked for the same horse liver isoenzyme [40], one would expect P to act as a mixed-type inhibitor of B [41]. The distinction is not

Table 2
Apparent pK_a values of k_{cat} and k_{cat}/K_m in catalyzed oxidation of *S*-1-phenylethanol or reduction of acetophenone. Apparent pK_a values were extracted after curve-fitting of functions for one or two titratable groups. See the Section 2 for details.

	Oxidation of *S*-**5**			Reduction of **6**		
	Wild-type		H39N	Wild-type		H39N
Parameter	pK_{a1}	pK_{a2}	pK_{a1}	pK_{a1}	pK_{a2}	pK_{a1}
k_{cat}	7.3 ± 0.06		7.7 ± 0.04	6.2 ± 0.7	7.4 ± 0.5	7.3 ± 0.1
k_{cat}/K_m	6.2 ± 0.06	8.4 ± 0.2	7.9 ± 0.04	7.3 ± 0.3		8.3 ± 0.3

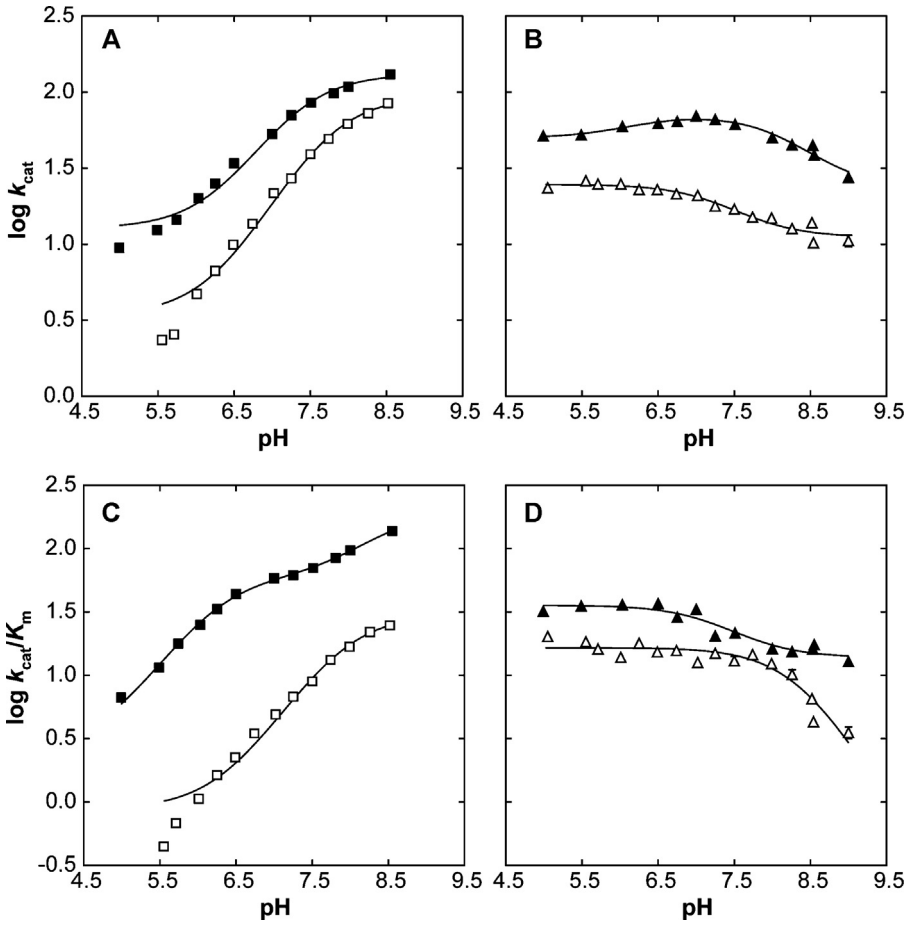

Fig. 3. pH-dependence of k_{cat} and k_{cat}/K_m in the oxidation of *S*-1-phenylethanol or reduction of acetophenone. The wild-type ADH-A is represented by filled symbols and the H39N ADH-A mutant by unfilled symbols. See Table 2 for determined pK_a values. (A) pH-dependence of k_{cat} for *S*-**5**. The turnover numbers increase with increasing pH in the oxidation for both enzyme forms, with a slight shift in the pH-dependence towards higher pH values by the H39N mutation. (B) The k_{cat} of the reduction of **6** displays a maximum around pH 7 for the wild-type catalyzed reactions resulting in two apparent acid constants. The more acidic of these pK_a values appears to be lost as a result of the H39N mutation. (C) k_{cat}/K_m for the oxidation reaction increases with increasing pH similar to k_{cat}, but again, the wild-type ADH-A displays two pK_a values while the H39N mutant only appears to depend on one titrated group in the tested pH range. The remaining pK_a in the H39N-catalyzed reaction seems to be shifted towards higher pH. (D) For the reduction reaction k_{cat}/K_m decreases with higher pH, with the pK_a value of the H39N mutant shifted towards higher pH as compared to the wild type.

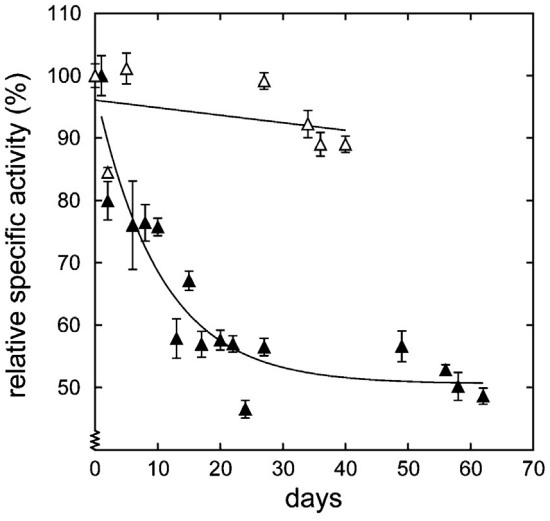

Fig. 4. Effect of zinc addition on retaining enzyme activity. The activity of wild-type ADH-A decreases over time when stored in 4 °C in zinc-free buffer to a level of approximately 50% over a time period of 60 days (filled symbols). Storing ADH-A in buffer containing 10 μM zinc sulfate (unfilled symbols) stabilizes the enzyme, retaining approximately 95% after 30 days of storage.

straight-forward, however, in that the order of substrate binding (A before B or possibly, *vice versa*) has not been unequivocally determined from direct binding studies. The relative affinities, however, suggest that A does bind before B in ADH-A (compare K_1 and K_3 in Table 4).

Increasing the pH to 8.0 changes the inhibition pattern so that NADH now acts as a *mixed-type* inhibitor of NAD^+ (Table 3, Fig. 6B). In order to explain this observation an isomerization step of the free enzyme ($E \leftrightarrow E^*$) has to be invoked and the resulting model may be described by an Iso Theorell–Chance mechanism [41] (Fig. 5C). Clues to the actual structural meaning of this invoked isomerization could be found from comparisons with the horse liver isoenzyme. It has been firmly established that the horse liver ADH partitions

Table 3
Product inhibition at pH 7 and 8. A, B, Q and P are represented by NAD^+, *S*-**5**, NADH and **6** respectively. Schematic representations of the proposed model mechanisms are presented in Fig. 5B and C. The double-reciprocal plots are presented in the Supplementary Information.

	pH 7		pH 8	
	Varied substrate		Varied substrate	
Inhibitor	A	B	A	B
P	Mixed type	Competitive	Mixed type	Competitive
Q	Competitive	Mixed type	Mixed type	Mixed type

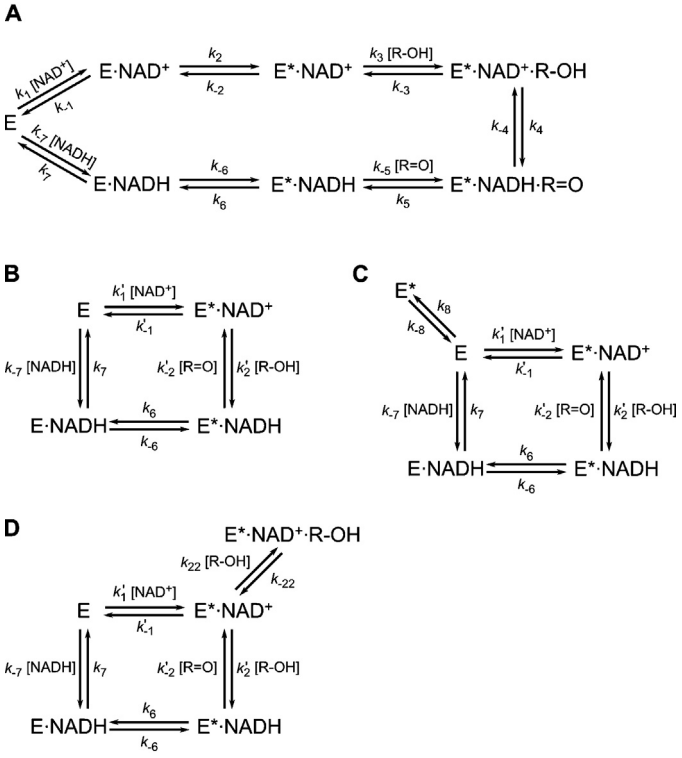

Fig. 5. Kinetic mechanism models based on product inhibition and pre-steady state kinetics. (A) The full model including enzyme isomerization steps triggered by nucleotide binding, as previously described for the horse liver enzyme [44]. (B) The Theorell–Chance (hit-and-run) mechanism which best describes the product inhibition results for the oxidation of *S*-**5** at pH 7.0 where NADH and **6** act as competitive inhibitors of NAD^+ and *S*-**5**, respectively. The apparent rate constants $k_{2'}$, $k_{-2'}$ are: $k'_2 = k_3k'_4/\left(k_{-3}+k'_4\right)$ and $k'_{-2} = k_{-3}k'_{-4}/\left(k_{-3}+k'_4\right)$; $k'_4 = k_4k_5/(k_{-4}+k_5)$ and $k'_{-4} = k_{-4}k_{-5}/(k_{-4}+k_5)$.
(C) The Iso Theorell–Chance mechanism which agrees with the product inhibition data at pH 8.0 where NADH acts as a mixed-type inhibitor of NAD^+. The difference between (B) and (C) is an added enzyme isomerization step that is substrate *independent*. (D) Model (C) with an added step for non-productive binding of the alcohol substrate. The determined values of rate and thermodynamic constants are given in Table 4.

between two distinct conformations where a more closed form is stabilized upon binding of the coenzyme [42–44]. In the closed form the active site and the catalytic zinc ion are shielded from solvent rendering the micro-environment more hydrophobic. The ternary enzyme-substrate complex also stabilizes binding modes of the second substrate that facilitate hydride transfer [45]. In the closed form the binding site for the coenzyme is inaccessible implying an ordered binding mechanism in which the cofactor binds to the enzyme in its open state (E) thereby favoring the transition to the closed state (E*) as schematically drawn in the model in Fig. 5A. The mechanism model in Fig. 5A is based on the model described for the horse liver enzyme [44].

How to link these movements in the horse liver enzyme to the observed shift in the inhibition pattern of the bacterial ADH-A is not obvious but the crystal structures of ADH-A provide some space for speculation. There are two available crystal structures determined at different pH values, 2xaa at pH 8.5 and 3jv7 at pH 5.5 [21]. Both of these structures describe the coenzyme-bound forms so it follows that there is no structural evidence for an "open" form of the ADH-A apoenzyme. A comparison of the crystal structures of ADH-A determined at pH 5.5 (3jv7) with that of the horse liver enzyme in the closed conformation (1lde) [46] demonstrates that although the sequence similarity of these two enzymes is poor in the corresponding regions of the active sites, the positions of the loops closing over the nucleotide binding sites are virtually superimposable between the two structures (Fig. 2C). In the closed conformation of the horse liver enzyme, the side-chain of Val294 comes in van der Waals contact with the pyridine ring of the bound coenzyme [45,47]. MD simulations have pinpointed this residue as part of a segment undergoing anticorrelated motions to that of the cofactor and thereby contributing to ground state activation of the substrates [48,49]. In ADH-A, the residue corresponding to Val294 is Ile271 (Fig. 2C). In the *R. ruber* enzyme this loop contains a non-conserved His residue, adjacent to Ile271. In both ADH-A structures, the N-δ of His272 forms a hydrogen bond with the backbone carbonyl oxygen of Val247 (Fig. 2D). Although, the crystallographic B-factors of the imidazole ring of His272 are relatively high, suggesting that this group is structurally flexible, it is conceivable that this interaction may contribute to stabilize the closed form also of the apoenzyme and that this interaction could be differentially affected by the differences in pH. This would require a conformational change back to the open state in order to form a new productive enzyme-cofactor complex. More studies are clearly needed to clarify the present observations of pH-dependent product inhibition.

The microscopic rates were analyzed by monitoring the transient changes in intrinsic protein tryptophan fluorescence upon binding of coenzyme or the NADH fluorescence during the redox chemistry. NAD^+ and NADH binding to ADH-A followed single exponential curves (Fig. 7C and D) where the observed rates (k_{obs}) were best modeled by a hyperbolic dependence of coenzyme concentration as described by Equation (5) (Fig. 7A and B). We also attempted to fit a linear one-state model (Equation (4)) to the data

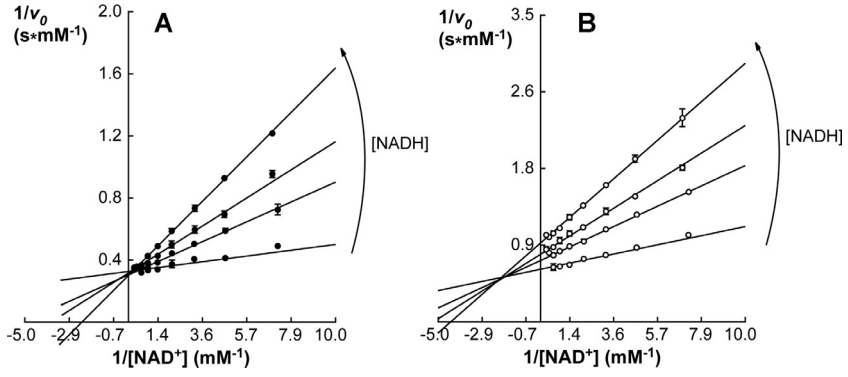

Fig. 6. Product inhibition of NADH versus NAD^+ at pH 7 and 8. Steady state kinetics of the pseudo-first order reaction of *S*-**5** (saturating concentration) and NAD^+ (varied concentrations) in the presence of increasing concentrations of NADH as inhibitor. The Michaelis–Menten equation was fitted to the experimental data. The fits are presented as double-reciprocal plots. (A) pH 7.0 results in competitive inhibition. (B) pH 8.0 displays mixed inhibition. Table 3 summarizes the product inhibition pattern of ADH-A at pH 7 and pH 8 for the reaction in the oxidative direction.

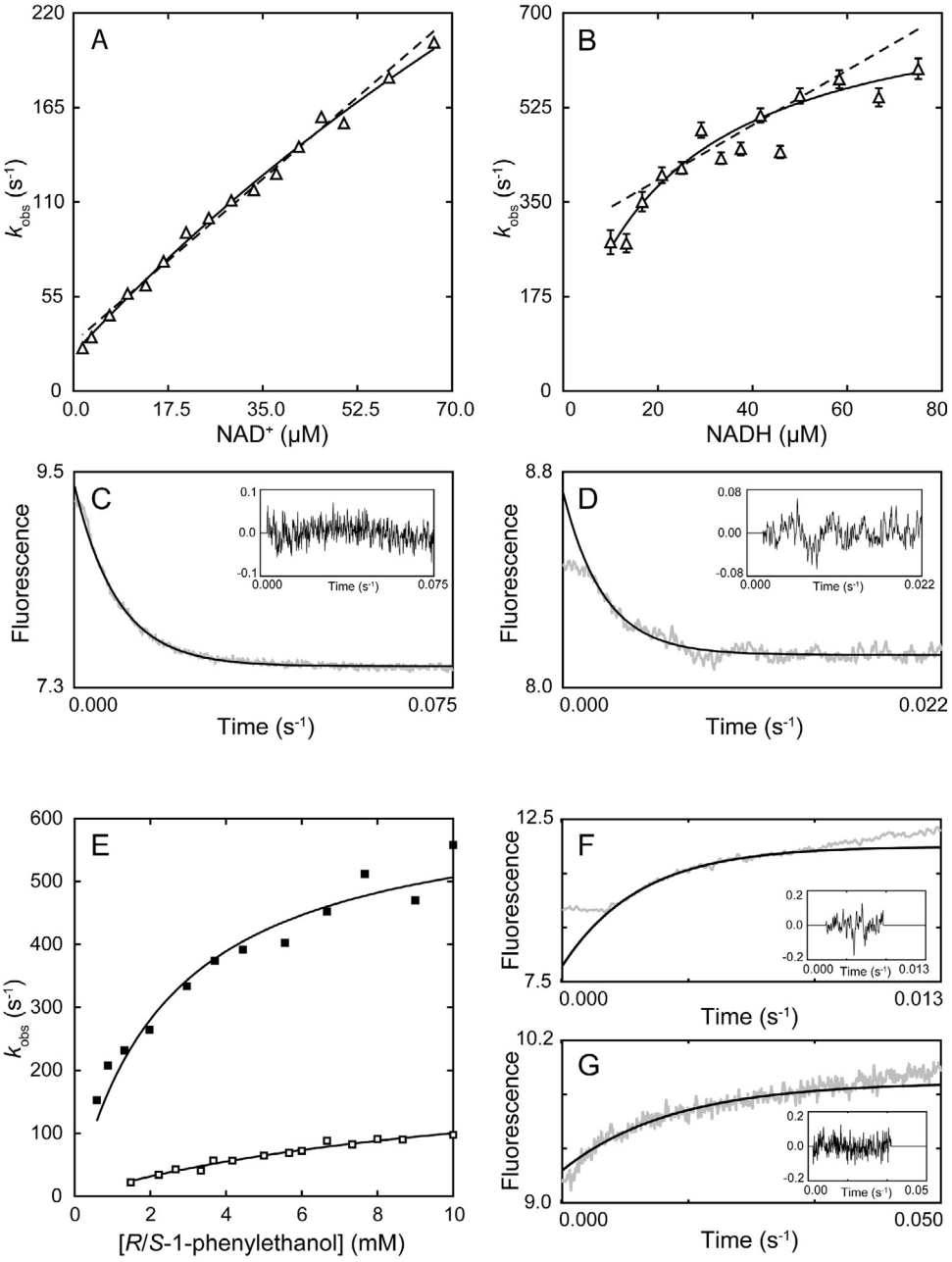

Fig. 7. Pre-steady state kinetics. Observed rates, k_{obs}, versus (A), [NAD^+] and (B), [NADH] Solid lines represent the fits to a two-state model (Equation (5)) and the dashed line to a one-state model (Equation (4)). Error bars represent standard deviations, $n \geq 8$. (C) and (D) show in grey averages of experimental traces ($n \geq 8$) of fluorescence decay in the presence of (C) 25 μM NAD^+ and 1.1 μM ADH-A, and (D), 25 μM NADH and 2.2 μM ADH-A. Solid black lines represent a single exponential fit to the data. (E) Substrate dependence of k_{obs} for the oxidation of *S*-**5** (filled squares) and *R*-**5** (unfilled squares). Solid lines represent the fits to Equation (6). (F) and (G) show in grey averages of experimental traces ($n \geq 8$) of fluorescence increase in the presence of (F) 4.4 mM *S*-**5**, 0.4 mM NAD^+ and 0.6 μM ADH-A, and (G), 5.7 mM *R*-**5**, 0.4 mM NAD^+ and 2.3 μM ADH-A. Solid lines represent a single exponential fit to the burst phase of the fluorescence traces. See Table 4 for determined values of kinetic parameters. Residual plots of the respective fits are shown in boxes.

Table 4
Microscopic rates and equilibria during catalyzed oxidation of 1-phenylethanol and reduction of acetophenone. Microscopic rates and thermodynamic constants were determined at pH 8.0 during pre-steady state or at steady state, as described in the Section 2. Numbering refer to the model mechanism in Fig. 5A. K_1 and K_7 are the dissociation constants of E•NAD^+ (k_{-1}/k_1) and E•NADH (k_7/k_{-7}), respectively. K_3 is the apparent dissociation constant of *S*- or *R*-**5** from the E*•NAD^+•**5** ternary complex and is the ratio k_{-3}/k_3.

Substrate	K_1 (μM)	k_2 (s^{-1})	k_{-2} (s^{-1})	K_3 (mM)	k_4 (s^{-1})	k_6 (s^{-1})	k_{-6} (s^{-1})	K_7 (μM)	k_{cat} (s^{-1})	K_m (mM)
S-**5**	240 ± 100	820 ± 300	22 ± 3	2.5 ± 0.5	630 ± 40	46 ± 200	710 ± 100	22 ± 20	80 ± 20	0.63 ± 0.05
R-**5**				12 ± 2	220 ± 30				0.45 ± 0.005	0.94 ± 0.04
6				–	–				36 ± 0.8	1.2 ± 0.09

which would describe the process of binding of the free enzyme (E) in the open state and coenzyme to form the binary complex in the closed states (E*•NAD(H)). This simpler model was, however, rejected after statistical analysis. The two-state model invokes rapid pre-equilibria of the binary E•NAD(H) complexes followed by subsequent isomerization steps from the open to closed conformations. The extracted parameters describe the dissociation constants of the binary complexes in the open state(s) (K_1 and K_7) and the rates of isomerization from the open to the closed state(s) (k_2 and k_{-6}) and back to the open state (k_{-2} and k_6) (Fig. 5A). It should be noted that the horse liver isoenzyme exhibits an identical kinetic behavior in its binding of the nicotinamide coenzymes [19,44]. The values of the microscopic rates and thermodynamic constants are presented in Table 4.

The NADH fluorescence increase when E•NAD$^+$ was rapidly mixed with either enantiomer of **5**, also proceeded as single exponential events followed by steady state slopes (Fig. 7F and G). The burst phase of the curves was analyzed to determine the rates of alcohol oxidation (k_4). The substrate dependencies of k_{obs} were in both cases hyperbolic allowing for determination of both the oxidation rates and the apparent dissociation constants (K_3) of the alcohols from the respective ternary complexes (Fig. 7E and Table 4). We were unable to detect any burst kinetics in the reduction of **6** preventing determination of k_{-4} and K_5 (cf. Fig. 5A). The reason for the lack of signal may be due to that the rate of hydride transfer from NADH to acetophenone is too fast (>1000 s^{-1}) to be detected outside the dead time of the equipment.

From the combined results from the steady state and transient kinetics it is clear that the rate-determining steps for the reduction of **6** and the oxidation of *S*-**5** are the isomerizations from the respective closed binary complex(es) to the corresponding open complex(es). The isomerization rate from the closed E*•NADH complex to the open complex (k_6) is approximately 50 s^{-1} which is in the same range as $k_{cat}^{S\text{-}\mathbf{5}}$ (80 s^{-1}) and k_{-2} has a value of 22 s^{-1}, also similar to $k_{cat}^{\mathbf{6}}$ (36 s^{-1}). It should be noted at this point that the corresponding isomerization step of the closed state of the binary complex of the horse liver enzyme and NAD$^+$ has also been shown to be rate-limiting in the catalyzed reduction of acetaldehyde [44].

We have, however, not been able to pinpoint the rate-determining step in the catalyzed oxidation of the *R*-**5** enantiomer from the transient kinetics studies. The slowest identified step is the described isomerization from the closed to the open binary E•NADH complex. This rate, however, is still 100-fold faster than $k_{cat}^{R\text{-}\mathbf{5}}$. One possible explanation is that this enantiomer can bind in different modes at the active site, with a distribution of productive and non-productive modes (Fig. 5D). The fact that the K_m value is significantly lower than the apparent dissociation constant (K_3) supports the idea of non-productive substrate binding. This would also affect the turnover number to the same degree but leave k_{cat}/K_m unaffected [50]. The determined k_{cat} value should therefore, by this argument, be underestimated and k_6 could possibly be rate-limiting also for the *R*-**5** oxidation. The fact that the same non-chiral product is formed in the reactions with either enantiomer of **5** also speaks in favor of that non-productive substrate binding is a reason to the relatively low $K_m^{R\text{-}\mathbf{5}}$. A (rate-limiting) step downstream of acetophenone formation would affect the reactions with *R*- or *S*-**5** equally. Isopropanol (**2**) is oxidized with approximately the same efficiency as *R*-**5** by ADH-A, as judged by the respective k_{cat}/K_m values (Table 1). The isopropanol oxidation, however, displays values of $k_{cat}^{\mathbf{2}}$ and $K_m^{\mathbf{2}}$ that are 100-fold larger than those for the *R*-**5** reaction. Isopropanol can be viewed as a phenyl-truncated derivative of **5**. Lacking the phenyl substituent is expected to result in poorer binding affinity at the ADH-A active site and thereby faster equilibration of binding modes. The larger turnover number and a relatively higher K_m of **2** indicate poorer stabilization of productive (and non-productive) ternary complexes. Hence, the determined low (apparent) values of k_{cat} and K_m would be increased if *R*-**5** was bound only in a productive mode.

4. Conclusions

The main reason for our group to study the enzymology of the *R. ruber* ADH-A was its potential as a biocatalyst. We have established the substrate scope and kinetic mechanism of a potentially important enzyme for biotechnological applications and the gathered results will provide important guidance in future efforts to tailor its function to suit a role as an efficient chemical catalyst. The data adds to previous knowledge on the catalytic function of class I alcohol dehydrogenases and demonstrates the functional relatedness between evolutionary distant relatives such as the *R. ruber* and horse liver isoenzymes. The fact that the catalytic efficiencies expressed as k_{cat} in both these cases are limited by structural isomerizations, emphasizes the notion that high turnover numbers are not strongly selected for in natural evolution but rather the catalytic efficiencies during non-saturating concentrations of substrates. Both these enzymes can be considered as efficient if comparing their k_{cat}/K_m values for their preferred substrates which are in the range of 10^5–10^6 s^{-1} M^{-1}. The findings that ADH-A catalyzes the regioselective oxidation of aryl-substituted vicinal diols place it as an important addition to the biocatalytic tool-box. The enantioselectivity between favoring *S*-**5** over *R*-**5** appears to be due to non-productive binding of the least preferred enantiomer. It follows that manipulating non-productive substrate binding by mutagenesis and directed evolution may be a new general route to enzyme variants displaying improved or altered stereoselectivities. The proven activity with diols **8** and **10** forms a baseline for improvement by upcoming directed evolution.

Acknowledgments

Plasmid pREP4-groESL was kindly provided by Dr. Martin Stieger (F. Hoffman-La Roche Ltd. Basel, Switzerland). The work was supported by Swedish Research Council (VR 621-2011-6055).

Appendix A. Supplementary data

Supplementary data associated with this article can be found, in the online version, at http://dx.doi.org/10.1016/j.molcatb.2013.10.023.

References

[1] T.D.H. Bugg, Nat. Prod. Rep. 18 (2001) 465–493.
[2] R.J. Kazlauskas, Curr. Opin. Chem. Biol. 4 (2000) 81–88.
[3] S. Panke, M. Held, M. Wubbolts, Curr. Opin. Biotechnol. 15 (2004) 272–279.
[4] J.C. Moore, D.J. Pollard, B. Kosjek, P.N. Devine, Acc. Chem. Res. 40 (2007) 1412–1419.
[5] H. Asako, M. Shimizu, N. Itoh, Appl. Microbiol. Biotechnol. 84 (2009) 397–405.
[6] L.M. Blank, B.E. Ebert, K. Buehler, B. Bühler, Antioxid. Redox Sign. 13 (2010) 349–394.
[7] G.W. Huisman, J. Liang, A. Krebber, Curr. Opin. Chem. Biol. 14 (2010) 122–129.
[8] D. Monti, G. Ottolina, G. Carrea, S. Riva, Chem. Rev. 111 (2011) 4111–4140.
[9] M. Hall, A.S. Bommarius, Chem. Rev. 111 (2011) 4088–4110.
[10] Y. Chen, C. Chen, X. Wu, Chem. Soc. Rev. 41 (2012) 1742–1753.
[11] A. Gurell, M. Widersten, Chembiochem 11 (2010) 1422–1429.
[12] D. Lindberg, M. de la Fuente Revenga, M. Widersten, Biochemistry 49 (2010) 2297–2304.
[13] Å. Janfalk Carlsson, P. Bauer, H. Ma, M. Widersten, Biochemistry 51 (2012) 7627–7637.
[14] P. Hoyos, J.-V. Sinisterra, F. Molinari, A.R. Alcántara, P. Dominguez De Maria, Acc. Chem. Res. 43 (2010) 288–299.
[15] W. Stampfer, B. Kosjek, C. Moitzi, W. Kroutil, K. Faber, Angew. Chem. Int. Ed. 41 (2002) 1014–1017.
[16] W. Stampfer, B. Kosjek, K.K. Faber, W. Kroutil, J. Org. Chem. 68 (2003) 402–406.
[17] H. Jörnvall, J.-O. Höög, H. von Bahr-Lindstrom, B.L. Vallee, Proc. Natl. Acad. Sci. U.S.A. 84 (1987) 2580–2584.
[18] M.F. Reid, C.A. Fewson, Crit. Rev. Microbiol. 20 (1994) 13–56.

[19] B.V. Plapp, Arch. Biochem. Biophys. 493 (2010) 3–12.
[20] M. Karabec, A. Łyskowski, K.C. Tauber, G. Steinkellner, W. Kroutil, G. Grogan, K. Gruber, Chem. Commun. 46 (2010) 6314–6316.
[21] B. Kosjek, W. Stampfer, M. Pogorevc, W. Goessler, K. Faber, W. Kroutil, Biotechnol. Bioeng. 86 (2004) 55–62.
[22] L.T. Elfström, M. Widersten, Biochim. Biophys. Acta 1748 (2005) 213–221.
[23] G.E. Dale, H.-J. Schönfeld, H. Langen, M. Stieger, Protein Eng. 7 (1994) 925–931.
[24] A.L. Davis, J. Keeler, E.D. Laue, D. Moskau, J. Magn. Reson. 98 (1992) 207–216.
[25] R.E. Hurd, B.K. John, J. Magn. Reson. 91 (1991) 648–653.
[26] L. Braunschweiler, R.R. Ernst, J. Magn. Reson. 53 (1983) 521–528.
[27] G. de Gonzalo, I. Lavandera, K. Faber, W. Kroutil, Org. Lett. 9 (2007) 2163–2166.
[28] K. Edegger, C.C. Gruber, T.M. Poessl, S.R. Wallner, I. Lavandera, K. Faber, F. Niehaus, J. Eck, R. Oehrlein, A. Hafner, W. Kroutil, Chem. Commun. 22 (2006) 2402–2404.
[29] K. Edegger, H. Mang, K. Faber, J. Gross, W. Kroutil, J. Mol. Cat. A: Chem. 251 (2006) 66–70.
[30] I. Lavandera, G. Oberdorfer, J. Gross, S. de Wildeman, W. Kroutil, Eur. J. Org. Chem. 15 (2008) 2539–2543.
[31] W. Stampfer, B. Kosjek, K. Faber, W. Kroutil, Tetrahedron: Asym. 14 (2003) 275–280.
[32] W. Stampfer, K. Edegger, B. Kosjek, K. Faber, W. Kroutil, Adv. Synth. Catal. 346 (2004) 57–62.
[33] R. van Deursen, W. Stampfer, K. Edegger, K. Faber, W. Kroutil, J. Mol. Catal. B: Enzym. 31 (2004) 159–163.
[34] H.W. Adolph, P. Maurer, H. Schneider-Bernlöhr, C. Sartorius, M. Zeppezauer, Eur. J. Biochem. 201 (1991) 615–625.
[35] H.W. Adolph, P. Zwart, R. Meijers, I. Hubatsch, M. Kiefer, V. Lamzin, E. Cedergren-Zeppezauer, Biochemistry 39 (2000) 12885–12897.
[36] R. Pietruszko, K. Crawford, D. Lester, Arch. Biochem. Biophys. 159 (1973) 50–60.
[37] R. Pietruszko, K. Voigtlander, D. Lester, Biochem. Pharmacol. 27 (1978) 1296–1297.
[38] L.A. LeBrun, B.V. Plapp, Biochemistry 38 (1999) 12387–12393.
[39] H. Theorell, B. Chance, Acta Chem. Scand. 5 (1951) 1127–1144.
[40] C.C. Wratten, W.W. Cleland, Biochemistry 2 (1963) 935–941.
[41] I.H. Segel, Enzyme Kinetics. Behavior and Analysis of Rapid Equilibrium and Steady-State Enzyme Systems, John Wiley and Sons, New York USA, 1975, pp. 653.
[42] H. Eklund, C.-I. Bränden, J. Biol. Chem. 254 (1979) 3458–3461.
[43] H. Eklund, J.-P. Samama, L. Wallén, C.-I. Brändén, J. Mol. Biol. 146 (1981) 561–587.
[44] V.C. Sekhar, B.V. Plapp, Biochemistry 29 (1990) 4289–4295.
[45] H. Eklund, B.V. Plapp, J.-P. Samama, C.-I. Bränden, J. Biol. Chem. 257 (1982) 14349–14358.
[46] S. Ramaswamy, M. Scholze, B.V. Plapp, Biochemistry 36 (1997) 3522–3527.
[47] H. Eklund, J.-P. Samama, T.A. Jones, Biochemistry 23 (1984) 5982–5996.
[48] J. Luo, T.C. Bruice, Proc. Natl. Acad. Sci. U.S.A. 99 (2002) 16597–16600.
[49] J. Luo, T.C. Bruice, Proc. Natl. Acad. Sci. U.S.A. 101 (2004) 13152–13156.
[50] A. Fersht, Structure and Mechanism in Protein Science, W. H. Freeman, New York, USA, 1999, pp. 114–116.